Saudi Pharmaceutical Journal 32 (2024) 102102

HOSTED BY

Contents lists available at ScienceDirect

Saudi Pharmaceutical Journal

journal homepage: www.sciencedirect.com

Original article

Antifibrotic effect of the P2X7 receptor antagonist A740003 against acute myocardial infarction-induced fibrotic remodelling

Noura Almusallam [a,b], Asma Alonazi [a,*], Anfal Bin Dayel [a], Abdullah Almubarak [c], Rizwan Ali [d], Wajd Althakfi [e], Rehab Ali [a], Nouf Alrasheed [a]

[a] Department of Pharmacology and Toxicology, College of Pharmacy, King Saud University, Riyadh 11451, Saudi Arabia
[b] Pharmaceutical Care Department, King Saud Medical City, Ministry of Health, Riyadh 11196, Saudi Arabia
[c] Experimental Surgery and Animal Laboratory, Prince Naif Bin Abdul Aziz Health Research Center, King Saud University, Riyadh 11451, Saudi Arabia
[d] King Abdullah International Medical Research Center, Medical Research Core Facility and Platforms, King Saud bin Abdulaziz University for Health Sciences, Ministry of National Guard Health Affairs, Riyadh 11481, Saudi Arabia
[e] Department of Pathology, College of Medicine, KSUMC, King Saud University, Riyadh 11451, Saudi Arabia

ARTICLE INFO

Keywords:
Myocardial infarction
P2X7-receptor
Fibrosis
TGF-β1/Smad
GSK-3β
A740003

ABSTRACT

Post-acute myocardial infarction (AMI) fibrosis is a pathophysiologic process characterised by activation of the profibrotic mediator, transforming growth factor-β (TGF-β). AMI is associated with a substantial increase in the levels of extracellular adenosine triphosphate (eATP), which acts on the purinergic P2X7-receptor (P2X7-R) and triggers an inflammatory response that contributes to myocardial fibrotic remodelling. P2X7-R has been implicated in several cardiovascular diseases; however, its role in the regulation of cardiac fibrosis remains unclear. Therefore, the current study aimed to determine the effect of the P2X7-R antagonist, A740003, on post-AMI fibrosis, via the profibrotic TGF-β1/Smad signalling pathway, and elucidate whether its effect is mediated via the modulation of GSK-3β. AMI was induced by surgical ligation of the left anterior descending coronary artery, Thereafter, animals were divided into groups: sham control, MI-untreated, MI-vehicle, and MI-A740003 (50 mg/kg/day) and treated for seven days accordingly. The heart weight/body weight ratio of untreated-ligated rats significantly increased by 15.1 %, creatine kinase-MB (CK-MB) significantly increased by 40 %, troponin-I levels significantly increased by 25.4 %, and lactate dehydrogenase significantly increased by 47.2 %, indicating myocardial damage confirmed by morphological changes and massive cardiac fibrosis. The protein expression of cardiac fibronectin, TGF-β1, and p-Smad2 were also upregulated by 143 %, 40 %, and 8 %, respectively, indicating cardiac fibrosis. The treatment of ligated rats with A740003 led to improvement in all the above-mentioned parameters. Overall, A740003 exhibits potential cardio-protective effects on post-AMI fibrotic remodelling in the animal model of AMI through P2X7-R blockade, possibly by downregulating the profibrotic TGF-β1/Smad signalling pathway and restoring GSK-3β phosphorylation. Altogether, treatment with A740003 could serve as a new cardioprotective strategy to attenuate post-AMI fibrotic remodelling.

1. Introduction

Cardiovascular disease (CVDs) is considered the most important cause of death worldwide based on its high morbidity and mortality rates (WHO, 2021). In fact, CVDs accounts for 32 % of all deaths globally. However, in Saudi Arabia, this figure exceeds 37 %. Acute myocardial infarction (AMI) accounts for 85 % of CVDs cases and has a global prevalence that is approaching 3 million (Mechanic et al.,

Abbreviation: AMI, Acute Myocardial Infarction; ATP, Adenosine Triphosphate; BBG, Brilliant Blue G; CK-MB, Creatine Kinase-MB; cTn-I, Cardiac Troponin-I; CVDs, Cardiovascular Diseases; DMSO, Dimethyl Sulfoxide; eATP, Extracellular Adenosine Triphosphate; ECM, Extracellular Matrix; ELISA, Enzyme-Linked Immunosorbent Assay; FL-IHC, Fluorescence Immunohistochemistry; LAD, Left Anterior Descending; LDH, Lactate dehydrogenase; P2X7-R, Purinergic 2X7-Receptor; p-GSK-3β, Phosphorylated-Glycogen Synthase Kinase-3β; p-Smad2, Phosphorylated Suppressor of Mothers Against Decapentaplegic; TGF-β1, Transforming Growth Factor-β1; TTC, Triphenyl Tetrazolium Chloride.

* Corresponding author at: Department of Pharmacology and Toxicology, College of Pharmacy, King Saud University, P.O. Box: 70474, Riyadh 11567, Saudi Arabia.
E-mail address: aaloneazi@ksu.edu.sa (A. Alonazi).

https://doi.org/10.1016/j.jsps.2024.102102
Received 13 March 2024; Accepted 13 May 2024
Available online 16 May 2024

2022; WHO, 2018). Post-AMI, the heart undergoes a healing process, which is defined as a series of pathological changes in structure and function of the myocardium that result in post-AMI cardiac remodelling. These changes can be divided into early remodelling, which includes ischaemia, necrotic cell death, and inflammation, and late remodelling, which is characterised by fibroblast activation in addition to the production and deposition of extracellular matrix (ECM) proteins (Zhao et al., 2020). Adverse ventricular remodelling, which ultimately progress to heart failure and death, is the main consequence (Frangogiannis, 2015).

Post-AMI fibrosis is a pathophysiological process typically initiated by inflammation or response to myocardium injury. This process is characterised by activation of the profibrotic mediator, transforming growth factor-β (TGF-β), which activates myofibroblast, the key cellular mediator of fibrosis. Myofibroblast functions as the primary collagen-constructing cell, thereby inducing excess accumulation of ECM for instance collagen and fibronectin (X. Yin et al., 2023). Numerous studies have explored the potential contribution of the TGF-β/Smad signalling pathway to the pathogenesis and progression of myocardium fibrosis. The TGF-β1 isoform is the preeminent pro-fibrotic cytokine recognized to date (Li et al., 2023). In particular, TGF-β1 performs a major role in cardiac pathophysiology by stimulating the release of profibrotic mediators; inhibiting the inflammatory response; promoting fibroblast activation, collagen synthesis, and ECM deposition; and inducing cardiac hypertrophy and fibrotic remodelling (Bagchi et al., 2016; Lovelock et al., 2005; Nicin et al., 2022; Shinde et al., 2017).

Purinergic receptors are extensively distributed in the heart and play different roles. These receptors are partitioned into two main families, P1 and P2, which are further subdivided into P2Y and P2X receptors that comprise seven subtypes (Shokoples et al., 2021b). P2X7-receptor (P2X7-R) is the last receptor subtype within the P2X family that has been characterised and is the most involved in the inflammatory process (Shokoples et al., 2021a). P2X7-R is an ATP-gated cation-selective ion channel that is stimulated by high concentration of extracellular adenosine triphosphate (eATP) (Shokoples et al., 2021b).

Although P2X7-R utilises ATP as a ligand, it presents a unique structure with low affinity for ATP and requires high eATP levels for activation (Shokoples et al., 2021b). As high levels of eATP are only present in response to tissue injury, the required concentration of eATP to activate P2X7-R is not present under normal physiological conditions (Eltzschig et al., 2012). Unlike other P2X receptors, P2X7 is unique because its downstream signalling is coupled to proinflammatory cascades (North, 2002). Therefore, in AMI, the levels of eATP released from ischaemic cardiomyocytes increase substantially, acting as a neurotransmitter on the purinergic P2X7-R (Sutton et al., 2017; Verkhratsky & Burnstock, 2014); mediating NLRP3 inflammasome formation and activation, which subsequently promote the activation and release of proinflammatory cytokines; triggering the inflammatory response that contributes to myocardial fibrotic remodelling; and leading to impaired cardiac function (Sandanger et al., 2013; Shokoples et al., 2021a). The inhibition of P2X7-R can limit the infarct area by preventing the development of the NLRP3 inflammasome (Barth et al., 2010). Several molecules have been established to block the P2X7-R action (De Marchi et al., 2016). Among them, the competitive cyanoguanidine derivative, A740003, exhibited the highest potency, selectivity, and specific antagonist activity for both rat and human P2X7-R (Honore et al., 2006).

Glycogen synthase kinase-3 (GSK-3) is a serine/threonine protein kinase that phosphorylates cellular substrates and modulates different cellular functions. The GSK-3 family involves two isoforms, GSK-3α and GSK-3β. Both isoforms are distributed equally within cardiomyocytes; however, GSK-3β has a higher activity in cardiomyocytes than the other isoform. GSK-3β regulates many crucial intracellular signalling pathways and has been implicated in various diseases, including AMI (Lal et al., 2015). However, the molecular mechanisms of GSK-3β regulation are complex and not fully understood. Based on accumulating evidence, GSK-3β negatively regulates TGF-β1/Smad signalling, thereby suppressing fibrotic gene expression (Guo et al., 2017; Lal et al., 2014). Several studies have investigated the link between P2X7-R activation and GSK-3β modulation in neuronal cells (Ortega et al., 2010), cancer cells (Amoroso et al., 2015; Zhang et al., 2019), and inflammation (Adinolfi et al., 2018). However, to date, no published data have revealed this link in cardiac myocytes. P2X7-R has also been implicated in several cardiovascular diseases; however, its role in regulating cardiac fibrosis remains unclear. Thus, the current study aimed to verify the possible cardioprotective effect of the P2X7-R antagonist, A740003, on post-AMI fibrosis, via the profibrotic TGF-β1/Smad signalling pathway. Moreover, whether the effect of A740003 is mediated via the modulation of GSK-3β was examined as a possible link.

2. Materials and methods

2.1. Chemicals

A740003 (#HY-50697), Evans blue stain (#HY-B1102), and triphenyl tetrazolium chloride (TTC) stain (#HY-D0714) were purchased from MedChemExpress (NJ, USA). Anti-phosphorylated-GSK-3β (p-GSK-3β (ser9) (#MBS9600628) was obtained from MyBiosource® (San Diego, USA); P2X7 antibody (#AF4626) was acquired from Affinity Biosciences (Cincinnati, USA); p-Smad2 antibody (phosphoS467) (#ab53100) and anti-fibronectin (#ab199056) were obtained from Abcam® (Boston, USA); and TGF-β1 antibody (#K003238P) was obtained from Solarbio® Life sciences (Tongzhou, China). The housekeeping loading control antibody, β-actin (mAbGEa) (#MA1.744), was obtained from Invitrogen® by Thermo Fisher Scientific (Waltham, USA). Alexa Fluor 488-conjugated Goat Anti-Rabbit IgG (H&L) secondary antibody (#A-11034) for immunostaining and HOECHST 33342 fluorescent stain of DNA and nuclei (#H3570) were purchased from Life Technologies (Thermo Fisher Scientific Corporation, Waltham, USA).

2.2. Experimental animals

A total of thirty-two adult male Wistar albino rats (250–330 g) were obtained from the Animal Care Center at the College of Pharmacy, King Saud University, Riyadh, Saudi Arabia. Rats were handled daily and appropriately housed in special cages under controlled standard temperature (25 ± 2 °C), humidity (40–60 %), and under 12 h light/dark cycles. The animals were accustomed to adapting to laboratory conditions for one week before initiation of the experimental procedure. During the experiment, rats were administered standard rodent maintenance chow and tap water *ad libitum*. All experimentations were performed in accordance with the Experimental Animal Ethics Committee Acts of King Saud University Institutional Research Ethics Committee (REC) (Ref. NO: KSU-SE-21–81) and the accepted international standards for handling experimental animals.

2.3. Experimental induction of AMI

The surgical procedures were performed at the Experimental Surgery and Animal Laboratory/Prince Naif Health Research Centre. Initially, rats were anaesthetised via inhalation of sevoflurane liquid (2–4%). As shown in Fig. 1, the surgical side was prepared by shaving the chest and disinfecting the area with an iodine solution. The rat was placed on a homeothermic blanket system to maintain its body temperature while lining the right side. Once steady breathing was confirmed, the rats were settled in the supine position, their chest cavity was opened, and a small transverse incision was made on the chest. The muscles were separated to expose the ribs, and an incision was made in the left intercostal space between the 4th – 5th ribs to expose the heart and locate the left anterior descending (LAD) coronary artery. A small, curved needle with a piece of suture was passed through the pathway of the LAD coronary artery and permanently ligated 2–3 mm from the apex of the heart. AMI was morphologically confirmed by regional cyanosis of the anterior wall of

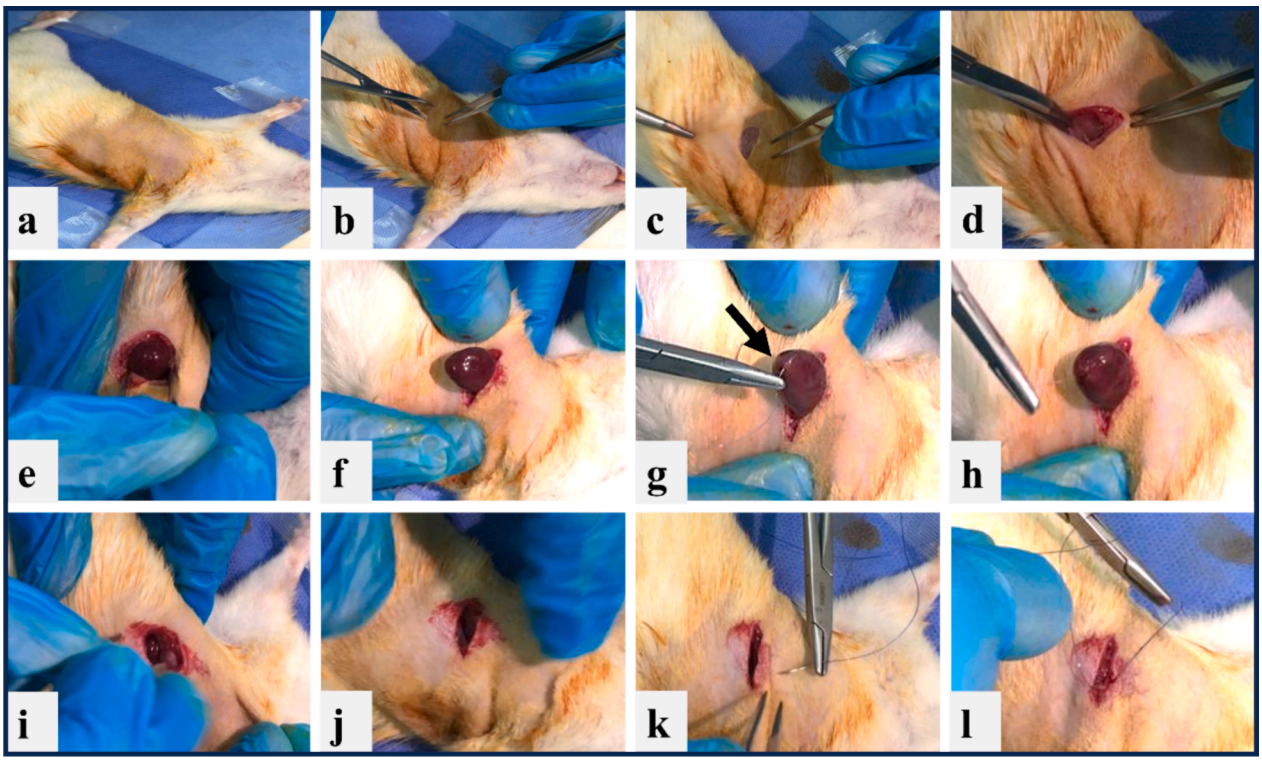

Fig. 1. Images of various stages in the surgical procedure for MI induction via permanent ligation of LAD coronary artery in rats (a-l). Arrow in (g) indicates the LAD coronary artery. Abbreviations: MI: Myocardial infarction, LAD: Left anterior descending.

the left ventricle (LV). The chest and skin incisions were closed layer by layer using sutures. The body temperature was maintained using a heating pad (Halim et al., 2018; Martin et al., 2022). After surgery, rats were returned to their cages, monitored for any abnormal signs or pain, and supplied water. Subsequently, the rats were intraperitoneally injected with the analgesic, flunixin as described previously (Liles & Flecknell, 1992), after surgery to prevent inflammation and relieve pain.

2.4. Experimental design

After one week of acclimatisation, 32 rats were weighed, with two rats housed per cage. The rats were then randomly allocated into four groups of eight and treated for seven days as outlined below (Fig. 2). ***Group I* ($n = 8$)**: Rats in the sham surgery control (Sham) underwent the same surgical procedure as rats in the other groups but without LAD coronary artery ligation or treatment, thereby serving as a negative control to exclude any effects that might occur due to this placebo surgery. ***Group II* ($n = 8$)**: Rats in the myocardial infarction untreated group (MI) underwent LAD coronary artery ligation surgery without receiving any treatment, thereby serving as the positive control. ***Group III* ($n = 8$)**: Rats in the myocardial infarction plus vehicle group (MI + Vehicle) underwent LAD coronary artery ligation surgery and were intraperitoneally administered an equivalent volume of the drug vehicle daily according to their daily weight (2 ml/kg/day, intraperitoneally), from the day of surgery to day seven. ***Group IV* ($n = 8$)**: Rats in the myocardial infarction plus A740003 group (MI + A740003) underwent LAD coronary artery ligation surgery and were treated with A740003. A740003 was injected intraperitoneally at a previously validated dose of 50 mg/kg/day; this dose has been shown to exert a biological effect (Yin, Wang, et al., 2017; Yin, You, et al., 2017). The drug was dissolved in the

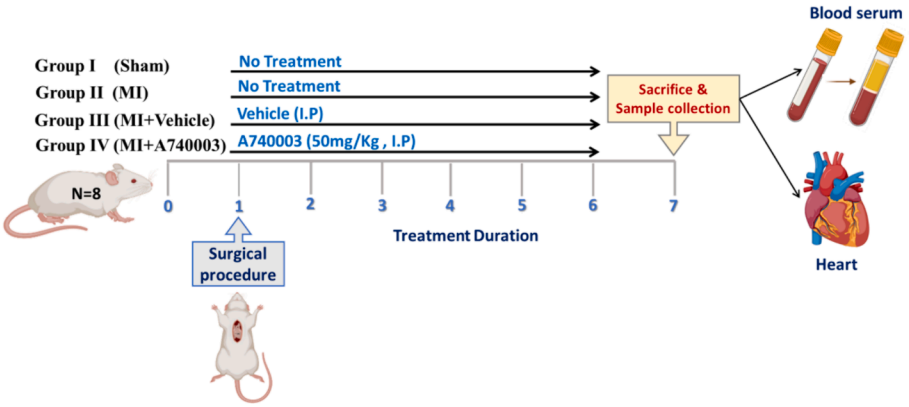

Fig. 2. Schematic of the experimental design, rat treatment, and timeline of the experimental process. Rats were distributed into four groups (n = 8): Control (underwent the same surgical procedure but without LAD coronary artery ligation or treatment; Sham), Myocardial infarction (MI), Myocardial infarction plus vehicle (MI + Vehicle), and Myocardial infarction plus A740003 (50 mg/kg/day) (MI + A740003). Once treatment period completed, blood samples collected and then serum were separated, and heart tissues were collected.

vehicle and administered daily according to the daily weight, from the day of surgery to day seven.

2.5. Blood sample collection

At the end of the treatment duration, all rats were re-weighed after overnight (12 h) fasting and anaesthetised using a sevoflurane inhalation system (2–4%). Trunk blood samples were harvested, allowed to coagulate, and processed via central centrifugation at 3000 rpm for 30 min at 4 °C to isolate and obtain the serum. Serum samples were apportioned into aliquots and stored at −80 °C for biochemical investigation.

2.6. Confirmation of successful ligation of LAD artery and assessment of the infarct area

To confirm the induction of infarction, the chest of rat was re-opened, and Evans Blue dye (1 % Evans Blue dye/normal saline) was used to stain the heart of 3–4 rats from each group. About 1 ml of the dye was injected into the renal artery and left for 2 min to stain the perfused parts of the myocardium blue. The nonperfused areas remained unstained. The hearts were then immediately excised, rinsed with normal saline, weighed, instantly frozen at −120 °C in liquid nitrogen for 10 s, and then serially cut into cross-sections from the apex to the base to create 1–2-mm-thick sections. The sections were then immersed in 1 % TTC stain dissolved in phosphate buffer solution at pH 7.4 and incubated for 10–20 min. The viable tissue with no infarction was stained red while the infarct region was left unstained (pale white). Following image capture, part of the heart slices was immediately frozen in liquid nitrogen and stored at −80 °C for immunoblotting analysis; the other part was immersed in 10 % buffered formalin fixative solution for histopathological staining and immunohistochemical studies.

2.7. Haemodynamic parameter measurements

In an appropriately warm, calm environment, the systolic (SBP), diastolic (DBP) blood pressure, heart rate (HR), body temperature (BT), and calculated mean arterial pressure (MAB) of rats were recorded every other day for 7 days using a CODA® Monitor non-invasive blood pressure system obtained from (Kent Scientific®, Torrington, USA). CODA uses volume–pressure recording sensor technology to identify alters in tail dimensions corresponding to SBP and DBP. Once placed in the restrainer, the rat was allowed to acclimate to the restrainer for 5 min before initiation of the measurement cycle. This period allowed the rats to relax and warm, which facilitated sufficient blood flow to the tail. The rats were warmed using heating pads on a restrainer platform during acclimation and measurement. Two tail cuffs [occlusion cuff (O-cuff) along with volume − pressure recording cuff (VPR-cuff)] were attached to the tail to initiate the blood pressure measurements session. After completion, the data were recorded.

2.8. Determination of body weight changes and calculation of the HW/BW ratio

The body weights of rats in each group were recorded daily from the day of surgery until the day of euthanasia. To evaluate the extent of cardiac hypertrophy, the heart weight to body weight (HW/BW) ratio was assessed as follows: HW/BW ratio = heart weight (mg)/body weight (g).

2.9. Serum biomarkers of cardiac injury

Serum levels of creatine kinase-MB (CK-MB) and cardiac troponin-I (cTn-I) were examined using specific ELISA kits (MyBioSource, San Diego, USA), according to the manufacturer's specifications. Serum lactate dehydrogenase (LDH) levels were measured spectrophotometrically using a commercially available kit (Stanbio Laboratory, Boerne, USA), according to the manufacturer's directions.

2.10. Histopathological studies

Samples of cross-sectional (transverse) heart tissue (obtained from at least three rats) were fixed in 10 % buffered formalin solution for 24 h, dehydrated in ascending grade of alcohol, embedded in paraffin, and sectioned at a thickness of 4 μm. The sections were de-paraffinized and rehydrated before staining with haematoxylin and eosin (H&E) and Masson's trichrome (MT), according to standard procedures (Chen et al., 2017). Haematoxylin was used to visualise nuclei (blue) while eosin was used to visualise the cytoplasm and connective tissue (shades of red or pink). MT resulted in a blue stain of collagen fibres. Histological images were captured using a Nikon DS-Ri2 camera (Nikon, USA).

2.11. Immunoblotting analysis of fibronectin, P2X7, TGF-β1, p-Smad2, and p-GSK-3β

Western blot analysis was performed to determine the protein levels of fibronectin, P2X7, TGF-β1, p-Smad2, and p-GSK-3β in the heart tissue lysate. Heart tissue proteins were extracted using lysis buffer (Sigma Chemical Co., USA) and quantified using a BCA protein assay kit (Thermo Fisher Scientific, USA), according to the manufacturer's instructions. The protein samples were calculated and adjusted to known equal concentrations (20 μg/μl), separated via 10 % SDS-PAGE as described by Laemmli (Laemmli, 1970), transferred onto polyvinylidene fluoride (PVDF) membranes (Bio-Rad, USA), blocked with 5 % bovine serum albumin (BSA) in Tris-buffered saline with Tween (TBST) buffer, and probed with primary antibodies (1:1000) followed by horseradish peroxidase (HRP)-conjugated secondary antibody (1:15,000). The protein signals were detected using enhanced chemiluminescence (ECL) and imaged using the ChemiDoc™ MP imaging system (Bio-Rad, USA). Blot density was quantified using Image J software. The expression levels of proteins were normalised to the loading control (β-actin) and then compared to the control group, whose value was fixed randomly to 1 and considered a fold of induction.

2.12. Analysis of P2X7-R, p-GSK3β, and fibronectin protein expression using fluorescent immunohistochemistry (FL-IHC)

FL-IHC staining of paraffin embedded heart sections was performed to detect three target proteins, P2X7-R, p-GSK3β, and fibronectin. The tissue samples were fixed with 10 % buffered formalin solution and embedded in paraffin. Thereafter, 4 μm sections were cut from the paraffin embedded heart tissues for subsequent experiments. Slide sample sections were de-paraffinized in xylene and rehydrated in a descending graded series of ethanol, according to standard procedures (Barth et al., 2010). Antigen retrieval was performed by heating the Tris-EDTA buffer at either 100 °C for 30 min or 60 °C overnight. After rinsing with Tris-buffered saline (TBS) and permeabilising buffer, the sections were blocked with 10 % foetal bovine serum (FBS) and 1 % bovine serum albumin (BSA) in TBS for 2 h at room temperature (25 ± 3 °C). Sections were subsequently incubated with primary antibodies (dilution 2:500) diluted in TBS with 1 % BSA overnight at 4 °C, rinsed for 5–10 min with TBS containing 0.025 % Triton, and incubated for 2 h with the secondary antibody (1:200) at room temperature in the dark. Finally, the slides were stained with HOECHST 33342 fluorescent stain (diluted in TBS, 1:1000) for DNA and nuclei for 20 min. The samples were analysed. Finally, images were acquired using a multichannel confocal laser scanning microscope (cLSM 780, Zeiss®, Germany) and processed using the Carl Zeiss ZEN 2011 (black edition) Version 7.0 software. The grey scale was adjusted to 100–225.

2.13. Statistical analysis

All data are expressed as mean ± standard error of the mean (SEM). Differences comparisons between the groups were performed using one-way analysis of variance (ANOVA), followed by a post-hoc multiple comparison test. Statistical analyses were implemented using GraphPad Prism 9 software (GraphPad Software Inc., USA). Differences were considered statistically significant at $P < 0.05$.

3. Results

3.1. Effect of A740003 on BW, HW/BW ratio, body temperature, and hemodynamic parameters including SBP, DBP, MAP and HR

After 7 days of MI induction, the body weights of rats in the MI and MI + Vehicle groups were found to significantly decrease ($P < 0.05$ and $P < 0.001$, respectively) compared with those of rats in the sham group. However, rats in the Sham group exhibited a normal increase in body weight until the end of the experiment (Table 1). The HW/BW ratio was measured as an indicator of cardiomyopathy development. As shown in Table 1, the HW/BW ratio was significantly increased in the ligated untreated group compared to the sham group ($P < 0.01$). The HW/BW ratio was significantly decreased in the group treated with A740003 compared to that in the ligation-untreated group ($P < 0.05$). SBP, DBP, MAP, HR, and body temperature readings were not found to significantly differ among the four groups.

3.2. Conformational studies of AMI induction

Evans blue and TTC staining were performed to confirm AMI occurrence and infarct size. Evans blue stained the viable perfused regions, whereas a pale stain was observed in the infarct region (Fig. 3a-c). To determine the cardioprotective effect of A740003 on cardiac injury biomarkers, serum levels of cardiac troponin I, CK-MB, and LDH were measured. The ligation untreated and ligation plus vehicle group had significant increases in the serum levels of CK-MB ($P < 0.01$; $P < 0.05$), LDH ($P < 0.01$; $P < 0.05$), and cTn-I ($P < 0.01$), respectively, compared with the sham group. However, treatment with A740003 ameliorated cardiac injury and significantly decreased LDH ($P < 0.01$) and cTn-I levels ($P < 0.05$) compared to ligation with no treatment (Fig. 3d-f).

3.3. Effect of A740003 on morphological and fibrotic changes

Changes in cardiac structure and myocardial fibrosis were assessed in at least three random heart tissue sections from each group using routine H&E and MT staining. Based on histological analysis, sham control rats had normal myocytes, exhibiting a syncytium of myocardial fibres with central nuclei (Fig. 4a). MT staining revealed normal distribution of fibrous tissue with no evidence of fibrosis (Fig. 4b). In contrast, a loss of myocyte normal-order structure, vacuolar degeneration resulting from ischaemia with anucleate pale myocytes, and moderate mononuclear cell infiltration were observed in heart sections from the infarction group (Fig. 4c). Areas of marked interstitial fibrosis were noted, with a significant increase in connective tissue in the infarction regions compared to that in the sham control (Fig. 4d). Similarly, cardiac myocytes in the infarction plus vehicle-treated group had a focal undulating (wavy) appearance with a decreasing diameter. Focal capillarisation and significant proliferation of fibroblasts with ischaemic modifications were also observed (Fig. 4e). Notably, areas of fibrosis and scar tissue with significantly increased connective tissue, similar to those in the MI group, were observed (Fig. 4f). Heart sections from rats with infarction and treated with A740003 displayed subtle improvement in myocardial cell degeneration, including a mild reduction in inflammation (Fig. 4g) and abnormal deposition of interstitial fibrous tissue (Fig. 4h).

3.4. Effect of A740003 on P2X7-R, fibronectin, TGF-β1, p-Smad2, and p-GSK3β protein expression

Immunoblotting was performed to measure the expression of target proteins in heart tissue lysates. The protein expression of P2X7-R increased in the MI and MI + Vehicle groups compared to that in the sham group; however, no significant difference was found (Fig. 5a). The myocardial protein level of fibronectin was markedly elevated by approximately three-fold in the MI and MI + Vehicle groups compared to that in the sham group ($P < 0.01$), indicating cardiac fibrosis. Conversely, MI + A740003 significantly suppressed fibronectin protein expression compared to that observed in MI ($P < 0.01$) and MI + Vehicle ($P < 0.05$) rats (Fig. 5b). The myocardial protein level of TGF-β1 was significantly elevated in the MI ($P < 0.001$) and MI + Vehicle ($P < 0.0001$) groups compared to the sham group, indicating cardiac remodelling and fibrosis. Treatment with A740003 significantly reduced

Table 1
Effect of A740003 on the HW/BW ratio, BW, Baseline BW, SBP, DBP, MAP, HR, and BT post-AMI induction.

	Sham	MI	MI + Vehicle	MI + Antagonist
HW	900.0 ± 40.50	894.0 ± 55.82	836.0 ± 35.86	874.0 ± 33.11
HW/BW	3.12 ± 0.03	3.59 ± 0.12**	3.38 ± 0.14	3.20 ± 0.04#
Baseline BW	288.8 ± 4.92	289.3 ± 8.48	278.0 ± 8.00	308.1 ± 7.49
BW	290.3 ± 7.57	254.9 ± 9.67*	240.6 ± 7.67***	270.6 ± 6.24
SBP	114.2 ± 10.23	111.7 ± 6.83	117.8 ± 5.38	113.3 ± 4.86
DBP	75.8 ± 1.86	77.43 ± 1.43	87.29 ± 1.97	90.75 ± 6.20
MAP	93.75 ± 2.25	91.83 ± 2.24	94 ± 2.30	102.3 ± 2.73
HR	354.5 ± 6.04	341.2 ± 12.41	338.2 ± 5.41	331.5 ± 3.60
BT	38.32 ± 0.17	38.25 ± 0.30	37.9 ± 0.23	38.16 ± 0.29

Summary of the haemodynamic parameters. Values are presented as mean ± SEM (n = 5), Group comparison was performed using one-way ANOVA followed by post-hoc Tukey-Kramer test;
* $P < 0.05$,
** $P < 0.01$,
*** $P < 0.001$, compared with the Sham group;
# $P < 0.05$, compared with the MI group. Abbreviations: Sham: Normal non-ligated, untreated rats; MI: Rats with myocardial infarction; MI + Vehicle: Rats with myocardial infarction and treated with the vehicle; MI + A740003: Rats with myocardial infarction and treated with A740003. HW/BW ratio: Heart weight to body weight ratio; BW: Body weight; SBP: Systolic blood pressure; DBP: Diastolic blood pressure; MAP: Mean arterial blood pressure; HR: Heart rate; BT: Body temperature.

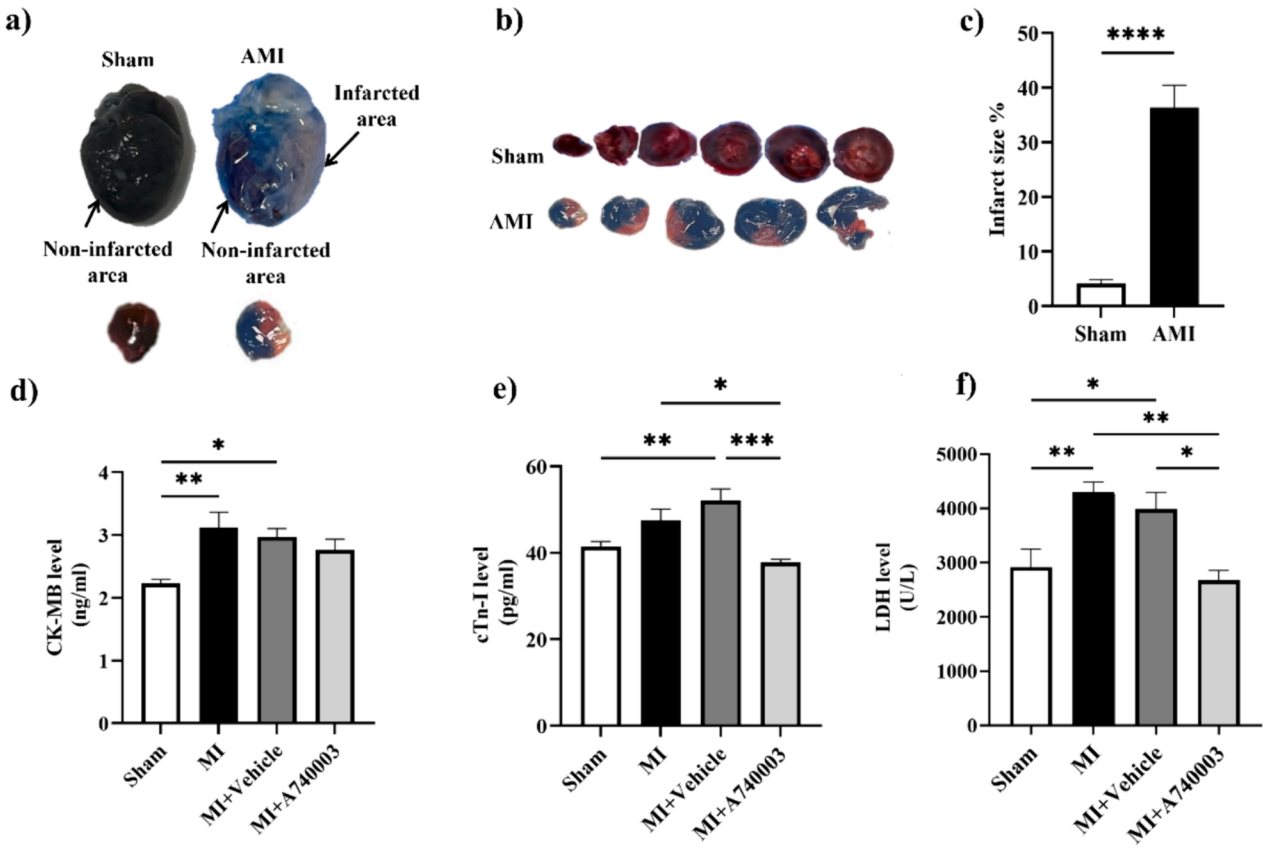

Fig. 3. Effect of permanent ligation on cardiac injury markers. (a) Representative images of a whole heart perfused with Evans-blue. (b) Representative images of transverse sections of Evans-blue-perfused and TTC-stained hearts. The dark blue area indicates the Evans blue perfused regions, red area indicates viable myocardium, and the white and ash regions indicate the infarct area. (c) Graphical presentation of infarct size in the Sham and infarction groups. Bar graph illustrating the serum level of (d) cTn-I, (e) LDH, and (f) CK-MB. Data are expressed as mean ± SEM, differences between groups were revealed using one-way ANOVA, followed by Tukey's comparison post-hoc test ($n \geq 5$), *$P < 0.05$; **$P < 0.01$; ***$P < 0.001$; ****$P < 0.0001$. Abbreviations; Sham: Normal non-ligated untreated rats; MI: Rats with myocardial infarction; MI + Vehicle: Rats with myocardial infarction and treated with vehicle; MI + A740003: Rats with myocardial infarction and treated with A740003. cTn-I: cardiac troponin I; LDH: lactate dehydrogenase; CK-MB: creatine kinase-MB. (For interpretation of the references to colour in this figure legend, the reader is referred to the web version of this article.)

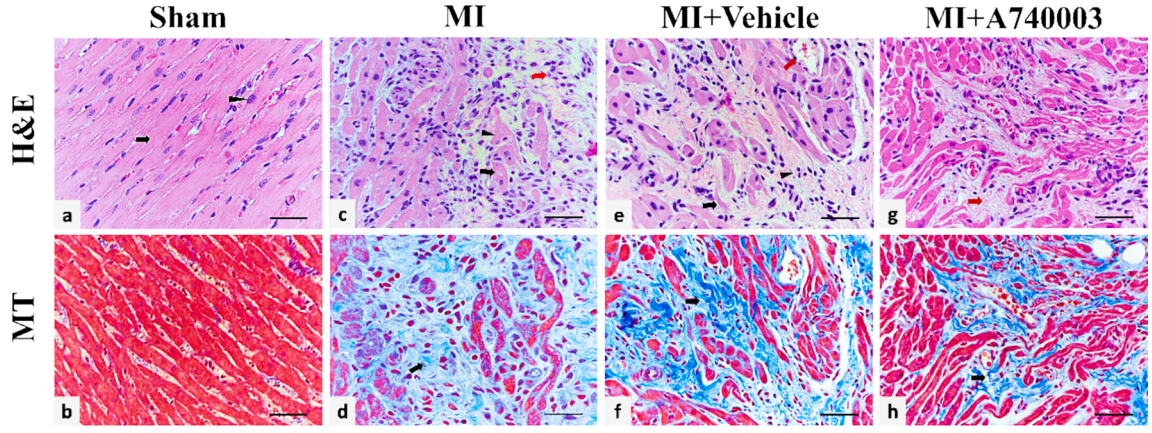

Fig. 4. Histopathological and fibrotic development in cardiac myocyte post-AMI. Representative photomicrographs of heart sections stained with H&E and MT illustrating the histopathological changes and highlighting the areas of fibrosis (Scale bar, 500 μm) (magnification x20). Sham: (a and b) H&E-stained sections of myocardial muscular fibres show a syncytium of myocardial fibres (black arrow) with central nuclei (arrowhead) while MT reveals no evidence of fibrosis. MI: (c and d) H&E staining highlighting the loss of the normal order structure of myocytes and vacuolar degeneration (black arrow) results from ischaemia with anucleate pale myocyte (arrowhead). Areas of marked interstitial fibrosis and moderate mononuclear cell infiltration were noted (red arrow), with MT indicating areas of fibrosis (black arrow) with a significant increase in connective tissue in the infarct areas of the heart tissue compared to the control. MI + Vehicle: (e and f) H&E-stained heart myocytes have an undulating (wavy) appearance with a decreasing diameter (black arrow). Focal capillarisation (red arrow), significant interstitial fibrosis, and proliferation of fibroblasts with ischeamic modifications are observed (arrowhead). MT indicates areas of fibrosis (black arrow) and scar tissue with significantly increased connective tissue. MI + A740003: (g and h) H&E staining highlighting less interstitial inflammation with minimal reduction in interstitial fibrosis (red arrow). A decrease in fibrosis density was confirmed by MT staining (black arrow). Abbreviations: Sham: Normal untreated rats with no infarction; MI: untreated rats with infarction; MI + Vehicle: vehicle-treated rats with infarction; MI + A740003: A740003-treated rats with infarction. (For interpretation of the references to colour in this figure legend, the reader is referred to the web version of this article.)

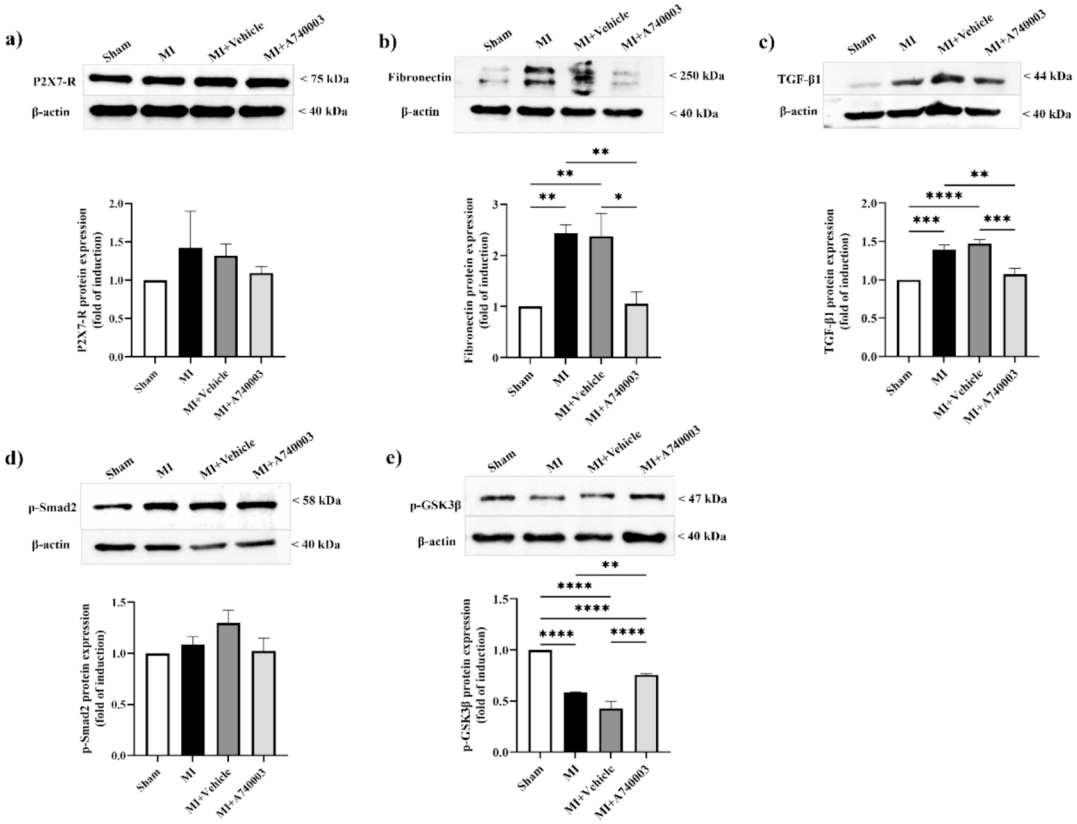

Fig. 5. Effect of A740003 on P2X7-R, fibronectin, TGF-β1, p-Smad2, and p-GSK3β protein expression post-AMI. (a) Representative immunoblot of P2X7-R protein expression (upper panel); Bar graph illustrates the quantitative analysis results of P2X7-R bands (lower panel). (b) Representative immunoblot of fibronectin protein expression (upper panel); Bar graph illustrates the quantitative analysis results of the fibronectin bands (lower panel). (c) Representative immunoblot of TGF-β1 protein expression (upper panel); Bar graph illustrates the quantitative analysis results of the TGF-β1 bands (lower panel). (d) Representative immunoblot of p-Smad2 protein expression (upper panel); Bar graph illustrates the quantitative analysis results of the p-Smad2 bands (lower panel). (e) Representative immunoblot of p-GSK3β protein expression (upper panel); Bar graph illustrates the quantitative analysis results of the p-GSK3β bands (lower panel). The relative values were quantified relative to those of the Sham group and expressed as a fold of induction. All data are presented as mean ± SEM (n ≥ 4 samples from different rats per group). Group comparisons were performed using one-way ANOVA followed by post-hoc Tukey's multiple comparisons test; *$P < 0.05$; **$P < 0.01$; ***$P < 0.05$; ****$P < 0.0001$. Abbreviations: Sham: Normal untreated rats with no infarction; MI: untreated rats with infarction; MI + Vehicle: vehicle-treated rats with infarction; MI + A740003: A740003-treated rats with infarction.

the protein expression of TGF-β1 compared with that observed with MI ($P < 0.01$) and MI + Vehicle ($P < 0.001$) (Fig. 5c). The p-Smad2 protein levels were not significantly elevated in the MI and MI + Vehicle groups compared to the sham group (Fig. 5d). AMI in all three groups (MI, MI + Vehicle, and MI + A740003) resulted in a marked reduction in p-GSK-3β protein level compared to that in the sham group ($P < 0.0001$), indicating enhanced activation of GSK-3β in the heart with infarction. However, treatment with A740003 significantly restored GSK-3β phosphorylation compared with that observed with MI ($P < 0.01$) and MI + Vehicle ($P < 0.0001$) (Fig. 5e).

3.5. FL-IHC to elucidate the effect of A740003 on P2X7-R, fibronectin, and p-GSK3β expression

The expression levels of P2X7-R, fibronectin, and p-GSK3β were detected in heart tissue via FL-IHC staining using specific antibodies against the target protein. P2X7-R was overexpressed in the expected infarct area of all ligated groups (MI, MI + Vehicle, and MI + A740003) compared to that in the Sham group (Fig. 6). The expression of fibronectin in heart sections from the MI and MI + Vehicle groups revealed a strong and massive immune reaction and recruitment of fibroblasts, indicating a marked increase in myocardial fibrosis compared to that in the Sham group. A740003 attenuated fibronectin expression compared to of MI and MI + Vehicle (Fig. 7). The expression of p-GSK-3β was decreased in the MI and MI + Vehicle groups compared to that in the Sham group. Treatment with A740003 restored the expression of GSK-3β phosphorylation (Fig. 8).

4. Discussion

In the current study, we used the novel P2X7-R antagonist, A740003, to block P2X7-R, which represents a significant advance in P2X7-R pharmacology. A740003 is a highly selective, specific, and potent antagonist of both rat and human P2X7-R (Donnelly-Roberts & Jarvis, 2007). Thus, the current study sought to determine the potential protective effect of A740003 on post-AMI fibrosis, which may occur via modulation of the profibrotic TGF-β1/Smad signalling pathway. Moreover, whether the effect of A74003 is exerted via modulation of GSK-3β was evaluated. Notably, the P2X7-R antagonist, A740003, attenuated cardiac fibrosis associated with post-MI remodelling.

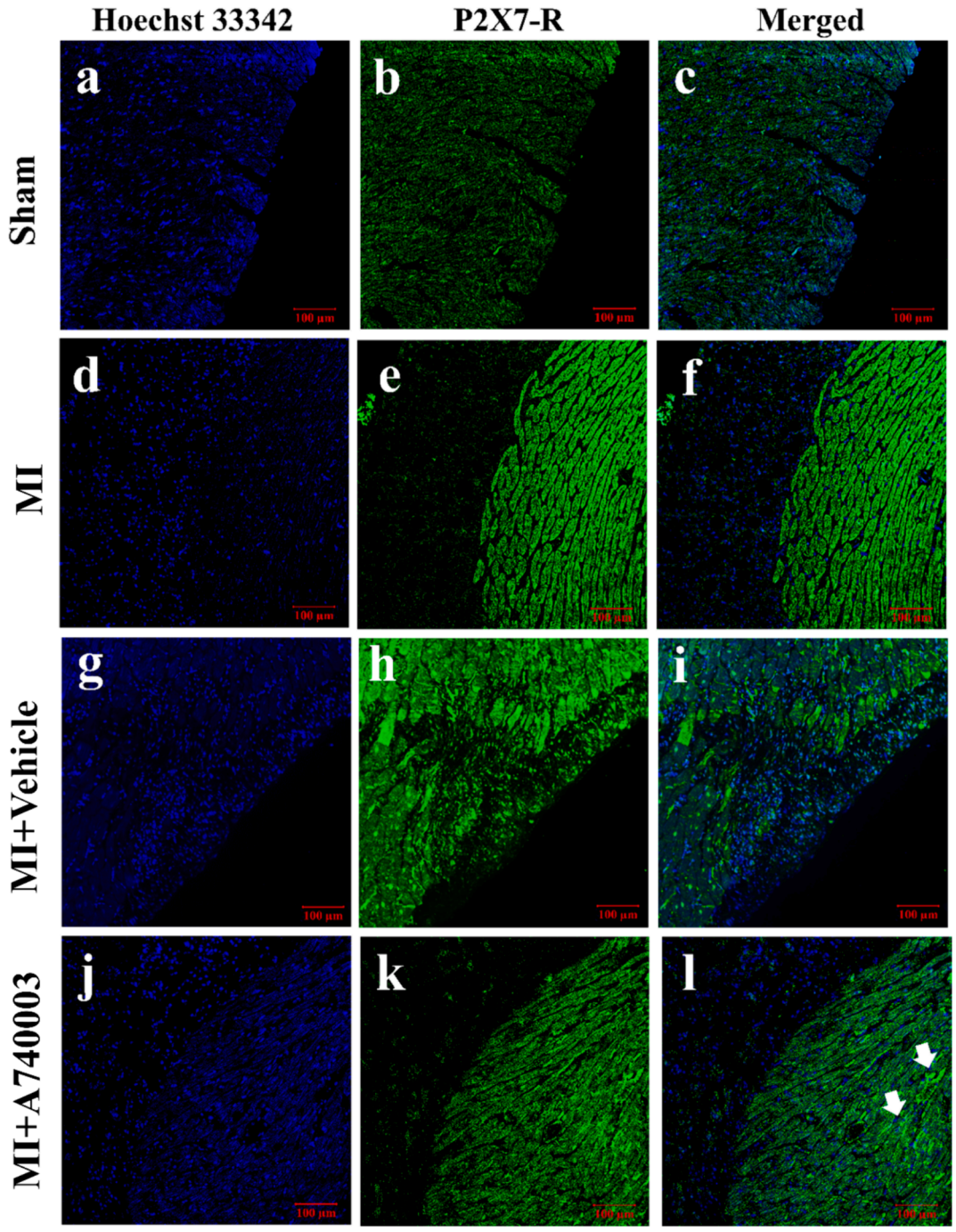

Fig. 6. FL-IHC of Nucleus and P2X7-R staining in heart sections of rats. (a-c) **Sham**; heart section of normal untreated rats with no infarction, (d-f) **MI**; untreated rat with infarction, (g-i) **MI + Vehicle**; vehicle-treated rats with infarction, (j-l) **MI + A740003**; A740003-treated rats with infarction. (a, d, g, & j) Hoechst 33,342 nucleus staining (blue); (b, e, h, & k) P2X7-R staining (green); and (c, f, I, & l) merged images. White arrows indicate overexpression of P2X7-R. All images were captured at a magnification of 20 x using a Zeiss LSM780 microscope system. Scale bar = 100 µm. (For interpretation of the references to colour in this figure legend, the reader is referred to the web version of this article.)

In a permanent ligation-induced AMI animal model, the body weight of rats with infarction reduced after surgical induction by LAD coronary artery ligation. This finding is consistent with that of previous studies, which found a postsurgical decrease in body weight (Gao et al., 2017; Yin, Wang, et al., 2017). A740003 was found to improve the body weight decline in rats with MI (Yin, Wang, et al., 2017). In addition, A740003 conferred similar benefits in an experimental mouse model of autoimmune myocarditis (EAM) (Zempo et al., 2015). The reduction in body weight could be attributed to postsurgical effects, such as malnutrition and dehydration. Moreover, existing findings revealed no effect of A740003 on blood pressure and heart rate after post-AMI induction. This outcome is consistent with that of previous studies on the P2X7-R inhibitor, A740003, which had similar effects on blood pressure and heart rate (Yin, Wang, et al., 2017; Zempo et al., 2015). However, previous studies have shown that treatment with the P2X7-R antagonists, Brilliant blue G (BBG) or oxidised ATP (oxATP), or knockdown of P2X7-R alleviates elevated SBP and HR after MI in rats (Liu et al., 2013; Tu et al., 2013), suggesting that P2X7-R contributes to neural sympathoexcitatory action and cardiac remodelling after MI.

Permanent surgical ligation of the LAD coronary artery is commonly

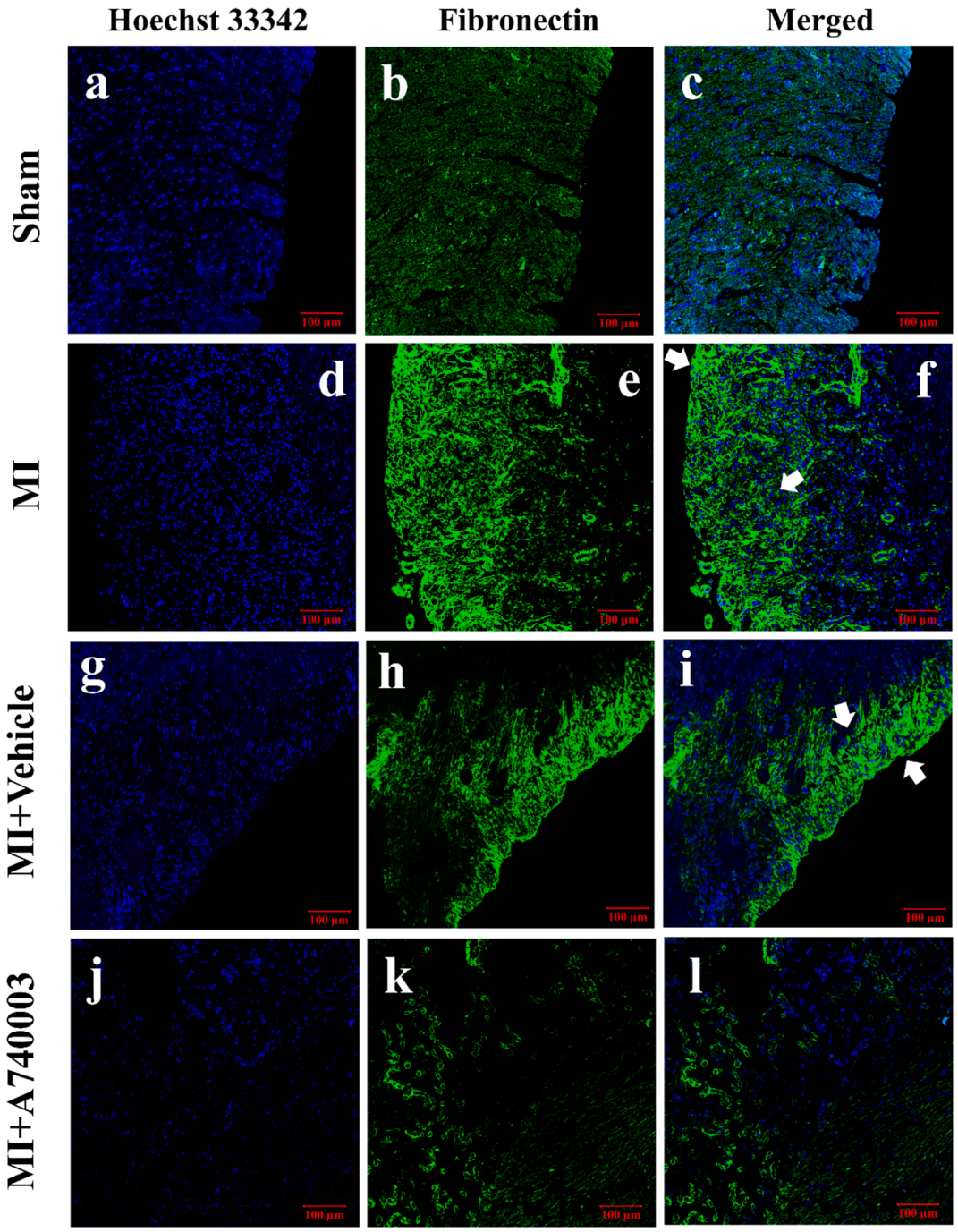

Fig. 7. FL-IHC of Nucleus and fibronectin staining in the heart sections of rats. (a-c) **Sham**; heart section of normal untreated rat with no infarction, (d-f) **MI**; untreated rat with infarction, (g-i) **MI + Vehicle**; vehicle-treated rats with infarction, (j-l) **MI + A740003**; A740003-treated rats with infarction. (a, d, g, & j) Hoechst 33,342 nucleus staining (blue); (b, e, h, & k) fibronectin staining (green); and (c, f, I, & l) merged images. White arrows indicate recruitment of fibroblasts, which reflects a marked increase in fibrosis in the MI and MI + Vehicle groups compared to the Sham group. All images were captured at a magnification of 20 x using a Zeiss LSM780 microscope system. Scale bar = 100 µm. (For interpretation of the references to colour in this figure legend, the reader is referred to the web version of this article.)

used to evaluate MI and long-term post-MI cardiac remodelling (Gao et al., 2017; Yin, Wang, et al., 2017). Permanent ligation is widely used to simulate approximately 30 % of patients with reperfusion failure or lack of timely reperfusion. This model enables assessments of the cellular and molecular mechanisms underlying tissue injury and wound healing. In addition, this model provides the precise location and extent of the coronary event due to direct observation of the ligated artery and the targeted area of infarction (Martin et al., 2022). Permanent ligation-induced AMI was confirmed by elevated serum levels of cTnI, CK-MB, and LDH, consistent with the findings of previous studies (Liu et al., 2013; Tu et al., 2013). These biomarkers are correlated with myocardial cell injury (Kemp et al., 2004). These elevated levels indicate increased cell membrane permeability or rupture, resulting in the leakage of these markers into circulation (Khadse et al., 2020). Consistent with previous studies on permanent ligation-induced histopathological changes (Chen et al., 2017; Michaud et al., 2020), AMI injury was confirmed by histopathological examination. Heart sections showed loss of normal myocyte structure and ischaemic vacuolar degeneration. In addition, an

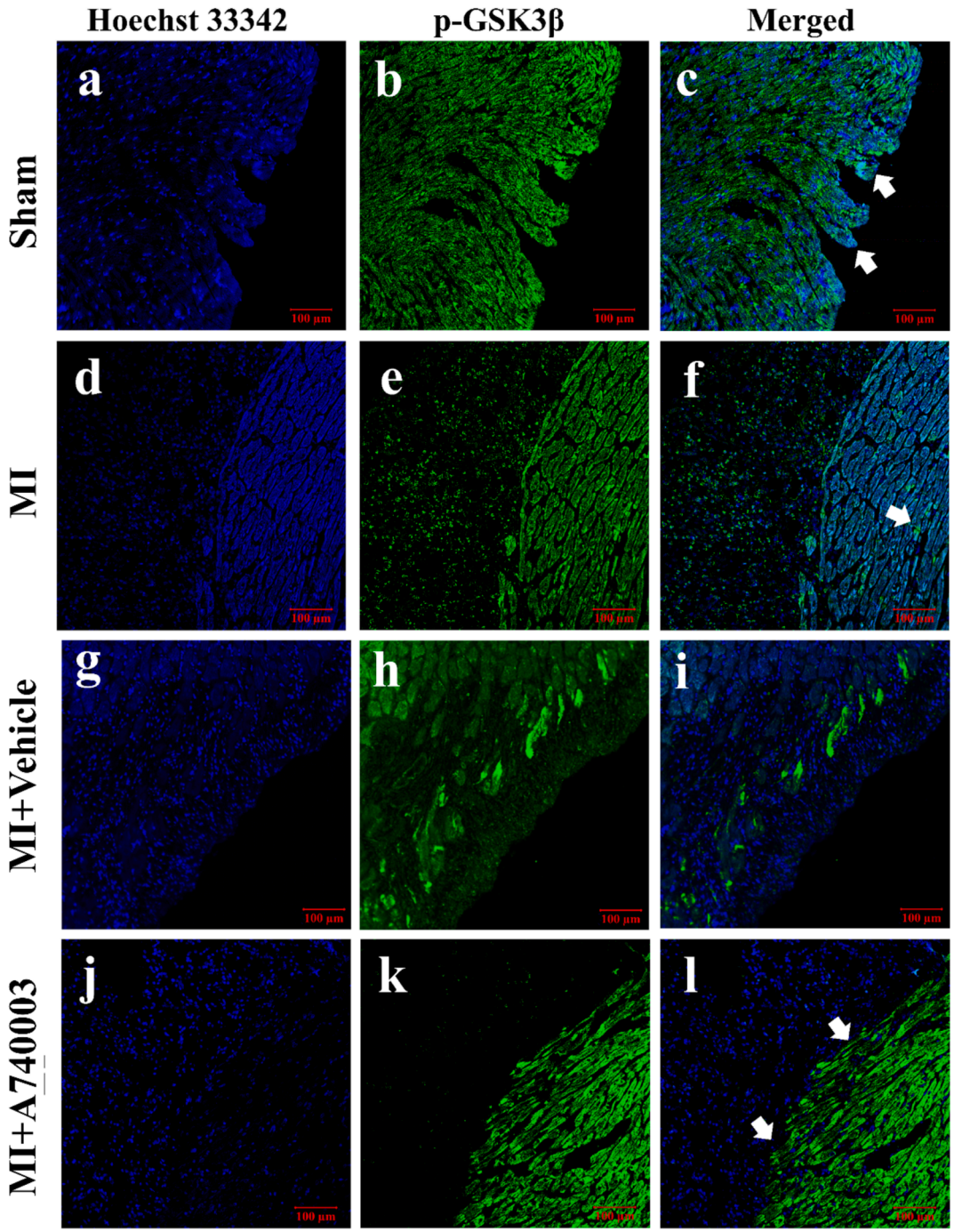

Fig. 8. FL-IHC of Nucleus and p-GSK3β staining in the heart sections of rats. (a-c) **Sham**; heart section of normal untreated rat with no infarction, (d-f) **MI**; untreated rat with infarction, (g-i) **MI + Vehicle**; vehicle-treated rats with infarction, (j-l) **MI + A740003**; A740003-treated rats with infarction. (a, d, g, & j) Hoechst 33,342 nucleus staining (blue); (b, e, h, & k) p-GSK3β staining (green); and (c, f, I, & l) merged images. White arrows indicate area of overexpression of p-GSK3β All images were captured at a magnification of 20 x using the Zeiss LSM780 microscope system. Scale bar = 100 µm. (For interpretation of the references to colour in this figure legend, the reader is referred to the web version of this article.)

area of marked interstitial fibrosis was observed. Treatment with A740003 significantly ameliorated the elevated serum levels of cTn-I and LDH, and to a lesser extent, CK-MB, in acute myocardial ischaemic rats. This improvement may reflect the cardioprotective effect of A740003 in the alleviation of myocardial ischaemic injury, which may be attributed to the anti-inflammatory effect of the P2X7-R antagonist (Yin, Wang, et al., 2017). Currently, data illustrating the effect of A740003 on cardiac injury biomarkers have not been published; however, P2X7-R knockdown or inhibition by BBG or oxATP treatment was found to reduce cTn-I, CK-MB, and LDH in a rat model of myocardial ischaemic injury (Liu et al., 2013; Tu et al., 2013). This amelioration was supported by histopathological studies in which treatment with A740003 resulted in a mild reduction in myocardial cell degeneration, including a mild-to-moderate reduction in interstitial fibrosis and inflammation. Although no published studies have revealed the effects of A740003 on the histopathological changes associated with AMI, a mouse model of experimental autoimmune myocarditis (EAM) revealed consistent findings for A740003 (Zempo et al., 2015).

Fibrosis was assessed according to the extent of replacement fibrosis. MT stain revealed a large infarct area, massive collagen fibre deposition,

and significant increase in connective tissue in the MI rats, which is associated with an increased HW/BW ratio in ligation-untreated rats. This result indicates cardiac hypertrophy and supports the necrosis, fibrosis, and accumulation of ECM. However, A740003-treated rats with infarction showed reduced abnormal deposition of collagen fibrous tissue and HW/BW ratio, aligning with previous findings (Yin, Wang, et al., 2017; Zapata-Sudo et al., 2014; Zempo et al., 2015). P2X7-R expression was detected via IHC in the sinoatrial node, atrial cardiomyocytes, as well as cardiac microvascular endothelial cells, but not in ventricular cardiomyocytes (Barth et al., 2010; Musa et al., 2009).

The role of P2X7-R antagonism by A740003 was previously investigated in a permanent ligation model of AMI (Yin, Wang, et al., 2017), indicating that MI induces marked P2X7-R activation 3–7 days post-MI in cardiac tissue homogenates of the LV. However, IHC of P2X7-R revealed that P2X7-R had a limited cellular distribution in hearts with infarction and mainly co-localised with macrophages rather than cardiomyocytes and interstitial cells. The inhibition of P2X7-R by A740003 is sufficient to conceal the earliest phases in post-AMI inflammatory cascades and ameliorates sympathetic sprouting via the NLRP3/ IL-1b signalling. Thus, P2X7-R may participate in the inflammatory process post-MI (Yin, Wang, et al., 2017). Other studies revealed increased P2X7 immunoreactivity, and mRNA and protein expression in myocardial ischaemic rats. However, treatment with the P2X7-R antagonists, BBG or oxATP, or knockdown of P2X7-R, decreased the expression levels of P2X7-R post-AMI (Liu et al., 2013; Tu et al., 2013). Moreover, antagonising or knocking out P2X7 or its subsequential effectors such as caspase-1 or NLRP3 reduced infarct size, enhanced cardiac function, and improved survival post-AMI in animal models via reduced IL-1β and IL-18 levels in the myocardium (Gao et al., 2017; Mezzaroma et al., 2011).

In this study, P2X7-R immunoreactivity and protein levels were assessed via FL-IHC and western blotting. Although western blotting revealed a non-significant moderate increase in the protein level of P2X7-R, FL-IHC displayed limited distribution of P2X7-R expression in the infarct area. Treatment with the P2X7-R inhibitor, A740003, reduced the expression level of P2X7-R in the cardiac homogenates of AMI rats; the same results were obtained via FL-IHC staining. These findings might be attributed to different explanations that are supported by previous studies; P2X7-R is suggested to be primarily located in non-cardiomyocytes (i.e., macrophages) rather than in cardiomyocytes and interstitial cells (Yin, Wang, et al., 2017). P2X7-R is also suggested to be expressed in the sinoatrial node, atrial cardiomyocytes, and cardiac microvascular endothelial cells, but not in ventricle cardiomyocytes (Barth et al., 2010; Musa et al., 2009).

P2X7-R performs a role in tissue fibrosis, such as the lung (Monção-Ribeiro et al., 2014) and liver (Tung et al., 2015). Recently, P2X7-R has been involved in several heart conditions, such as hypertension (Ji et al., 2012), EAM (Zempo et al., 2015), and AMI (Tu et al., 2013; Yin, Wang, et al., 2017). However, due to limited published data, the function of P2X7-R in cardiac fibrosis remains unclear.

According to a previous study, disruption of NLRP3 inflammasome formation using a P2X7-R antagonist pyridoxalphosphate-6-azophenyl-2′,4′-disulfonic acid (PPADS) in cardiomyocyte ameliorated cardiac remodelling, limited infarct size and myocardium cell death, and reduced cardiac fibrosis following AMI in a permanent ligation mouse model (Mezzaroma et al., 2011). Likewise, a recent study identified that P2X7-R inhibition by BBG reduced the mRNA and protein levels of profibrotic markers, resulting in significantly alleviated cardiac fibrosis and dysfunction, and attenuated dilated cardiomyopathy caused by pressure overload in a transverse aortic constriction (TAC) mouse model via suppressing NLRP3 inflammasome and its downstream effectors (Zhou et al., 2020).

TGF-β1 has been established as a profibrotic cytokine that negotiates tissue fibrosis incorporated with inflammation and tissue injury in post-MI remodelling (Khalil et al., 2017). Canonical TGF-β signalling phosphorylates and mobilises Smad2 and Smad3 transcription factors that regulate fibrotic process thru promoting gene expression (Khalil et al., 2017). Such result aligns with that of previous studies, which revealed that activation of NLRP3 inflammasome may regulate the IL-1β and IL-18 mediated TGF-β1/Smad2 signalling pathway, which is associated with LV remodelling (Jiang et al., 2021). The NLRP3/IL-1β inflammasome pathway itself was found to mediate TGF-β1- stimulated cardiac fibroblast activation (Zhou et al., 2020). Furthermore, a previous study reported that TGF-β1 induces cardiac fibroblasts (CFs) activation and differentiation into myofibroblasts resulting in ECM accumulations such as fibronectin and collagen. Also, they show that P2X7-R silencing in CFs ameliorates its effects on fibroblast activation (Zhou et al., 2020).

In the current study, post-AMI cardiac fibrosis in rats was revealed by elevated TGF-β1 and fibronectin protein levels. The protein levels of the profibrotic mediator, TGF-β1, and the essential component of the ECM, fibronectin, were significantly upregulated in rats with infarction. The same results were obtained for p-Smad2, one of the primary downstream mediators of TGF-β1. The current results are consistent with those of previous studies, in which elevated TGF-β1 and p-Smad2 protein levels were found in a coronary artery ligation model of AMI (Jiang et al., 2021; Qiu et al., 2018). Thus, activation of the TGF-β1/Smad2 signalling pathway may be associated with post-AMI fibrotic remodelling.

TGF-β1/Smad signalling strongly upregulates the expression of fibronectin and collagen type I and III in myocardial fibroblasts in ischaemic/reperfusion MI in mouse (Dobaczewski et al., 2010). Fibronectin was strongly upregulated in both heart sections and cardiac tissue homogenate seven days after MI (Konstandin et al., 2013). Recent research showed the role of Smad2 in infarct myofibroblasts, exhibiting stimulation of Smad2 signalling, based on nuclear localisation of p-Smad2, which is consistent with the current results. These studies, including the current findings, highlight an association between MI and ECM proteins and connective tissue accumulation, resulting in cardiac fibrosis.

Treatment with A740003 downregulated the levels of TGF-β1, p-Smad2, and consequently fibronectin. Although no data have been published on the role of A740003 in cardiac fibrosis, our findings are supported by earlier studies, in which P2X7-R blockade by BBG or PPADS was found to attenuate cardiac fibrosis and remodelling with reduced cell death (Mezzaroma et al., 2011; Zhou et al., 2020). Therefore, P2X7-R may participate in the pathogenesis of cardiac fibrosis mediated by the TGF-β-Smad signalling; targeting P2X7-R may attenuate the progression of cardiac fibrosis. Based on our results, the level of the p-GSK-3β protein was markedly downregulated in untreated rats with infarction, indicating GSK-3β activation, which is consistent with previous observation of Woulfe et al. These investigators found that the deletion of GSK-3β in cardiomyocytes protected against post-AMI remodelling, prevented an increase in fibrosis, and significantly reduced apoptosis the permanent LAD ligation MI model of cardiac-specific conditional GSK-3β knockout (KO) mice (Woulfe et al., 2010). Gomez et al. also used cardiac-specific transgenic GSK-3β-S9A mice with reperfused MI to reveal that serine 9 phosphorylation of GSK-3β is essential for cardiac protection from ischaemic postconditioning (Gomez et al., 2008).

Several studies have suggested contradictory effects in the relationship between post-AMI remodelling and GSK-3β activity. Double knock-in of phosphorylation-resistant GSK-3α/β in mice protects against pathological cardiac hypertrophy induced by isoproterenol stimulation, preserving myocardial contractile function and diminishing interstitial fibrosis (Webb, Nishino, et al., 2010). Phosphorylation and inactivation of GSK-3β have been observed in pathological stress remodelling in the mouse model of permanent LAD ligation MI (Webb, Sicard, et al., 2010). According to Lal et al., the deletion of GSK-3β from fibroblasts induce excessive fibrogenesis and scarring in ischaemic hearts, impairing cardiac function (Lal et al., 2014). Current finding indicates that treatment with A740003 in rats with infarction restored (increased) the p-GSK-3β activity, which reflects GSK-3β inactivation. This result highlights the potential role of GSK-3β signalling in P2X7-R-mediated cardiac fibrosis post-AMI. To our knowledge, the present study is the first to investigate

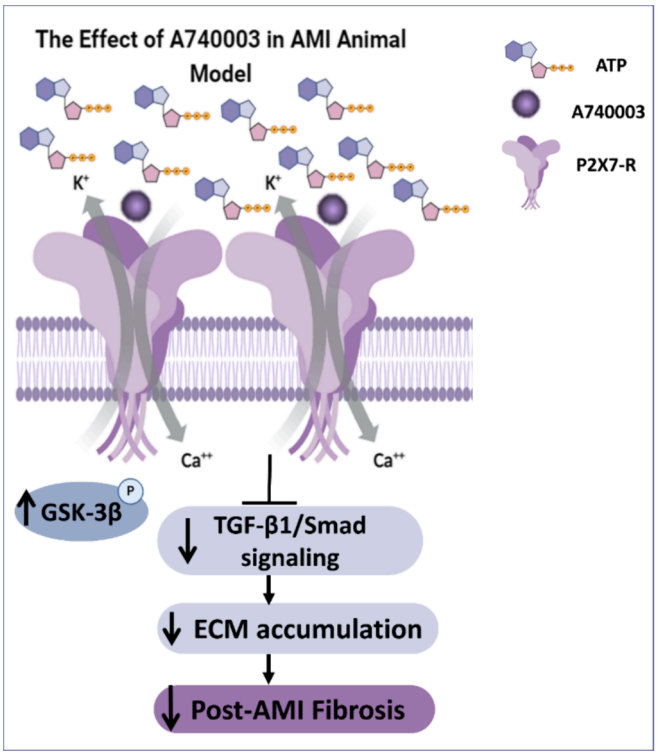

Fig. 9. Illustrative figure for the possible signalling pathways for the effect of P2X7-R antagonist (A740003) on post AMI fibrosis.

the effect of A740003 on myocardial fibrotic markers and p-GSK-3β (Fig. 9).

The rat model of AMI and LAD ligation surgery has several limitations. First, heart sections were analysed for only two groups (control Sham and MI rats) after TTC stating for confirmation of model induction. The reason for that as the heart sections shrink rapidly after staining with TTC, which affect the quality of images. Therefore, we use it for confirmation of model induction rather than to compare between all four groups. Second, the reduction in the number of animals after the initiation of the experimental procedure. We attributed this unexpected reduction in the number of animals to two main factors. One was the invasive nature of our experimental model of coronary ligation used for the induction of myocardial infarction. Although we took all possible measures to minimize the mortality rate, our protocol could not avoid the occasional death of an animal. Furthermore, for ethical reasons, we were obligated to exclude any animals that showed signs of illness or distress during the experimental period. A second factor was that the infarct size varied based on the ligation point. This may reflect technical issues associated with this invasive surgical procedure in the initial group of animals and can be considered an additional justification for ending the experiment with a smaller number of animals. However, the variation in infarct size among our animals was minor and sometimes negligible in some groups of animals and did not affect the data analyses, statistical power of the study, or consistency and reliability of the study outcomes. Accordingly, our focus on a subset of animals that shared representative infarct sizes could enhance the relevance, reproducibility, and interpretability of the research findings.

However, despite these limitations, the results of the current study indicate a key pathological effect of the P2X7 signalling pathway on post-infarction remodelling. Further investigations are required to reveal the effect of A740003 on the profibrotic signalling pathway using different experimental animal models, such as I/R injury. In addition, the role of p-GSK-3β in the post-AMI remodelling process needs to be confirmed.

5. Conclusions

Overall, the existing data strongly confirm for the first time that the P2X7-R antagonist A740003 exhibits potential cardioprotective effects on the progression of fibrotic remodelling associated with AMI. The underlying mechanism of A740003 may involve the P2X7-R-mediated TGF-β1/Smad signalling pathway. Furthermore, the potential link between P2X7-R activation and the TGF-β1/Smad signalling pathway may be attributed to GSK-3β phosphorylation. These results provide new insights into the role of P2X7-R in post-AMI remodelling. Therefore, targeting P2X7-R could be considered a cardioprotective strategy to treat and prevent the progression of fibrotic remodelling in patients with AMI.

CRediT authorship contribution statement

Noura Almusallam: Conceptualization, Data curation, Formal analysis, Investigation, Methodology, Software, Writing – original draft, Funding acquisition. **Asma Alonazi:** Conceptualization, Funding acquisition, Project administration, Supervision, Writing – review & editing. **Anfal Bin Dayel:** Conceptualization, Project administration, Supervision. **Abdullah Almubarak:** Methodology, Project administration. **Rizwan Ali:** Investigation, Methodology, Software, Visualization. **Wajd Althakfi:** Investigation, Methodology, Visualization. **Rehab Ali:** Investigation, Methodology, Project administration. **Nouf Alrasheed:** Validation, Writing – review & editing.

Declaration of Competing Interest

The authors declare that they have no known competing financial interests or personal relationships that could have appeared to influence the work reported in this paper.

Acknowledgements

The authors extend their appreciation to the Deputyship for Research & Innovation, “Ministry of Education” in Saudi Arabia, for partially funding this research through project number (IFKSUDR_H150). The authors thank the King Abdullah International Medical Center (KAIMRC) Medical Research Core Facility (MRCF) microscopy unit for providing experimental and technical support. The authors also thank Dr. Yasser Alshawakir for his help with the surgical procedures and Dr. Maha Alamin and Arwa Alsubait for their remarkable technical support.

Funding organisation

This work was supported by the Saudi National Institute of Health under grant agreement number [SNIH-RO-HRT01-2302-KSU-36360077]. The Deputyship for Research & Innovation, “Ministry of Education” in Saudi Arabia, partially funding this research through project number (IFKSUDR_H150).

Ethical consideration

The animal experimental protocol was assessed and approved by the Ethics Committee of King Saud University (KSU-SE-21-81).

References

Adinolfi, E., Giuliani, A. L., De Marchi, E., Pegoraro, A., Orioli, E., Di Virgilio, F., 2018. The P2X7 receptor: A main player in inflammation. In *Biochemical Pharmacology,* vol. 151, Biochem. Pharmacol., pp. 234–244, Doi: 10.1016/j.bcp.2017.12.021.

Amoroso, F., Capece, M., Rotondo, A., Cangelosi, D., Ferracin, M., Franceschini, A., Raffaghello, L., Pistoia, V., Varesio, L., Adinolfi, E., 2015. The P2X7 receptor is a key modulator of the PI3K/GSK3β/VEGF signaling network: Evidence in experimental neuroblastoma. In *Oncogene,* vol. 34, Issue 41, pp. 5240–5251. Doi: 10.1038/onc.2014.444.

Bagchi, R.A., Lin, J., Wang, R., Czubryt, M.P., 2016. Regulation of fibronectin gene expression in cardiac fibroblasts by scleraxis. Cell Tissue Res. 366 (2), 381–391. https://doi.org/10.1007/S00441-016-2439-1/METRICS.

Barth, K., Pfleger, C., Linge, A., Sim, J.A., Surprenant, A., Steinbronn, N., Strasser, R.H., Kasper, M., 2010. Increased P2X7R expression in atrial cardiomyocytes of caveolin-1 deficient mice. Histochem. Cell Biol. 134 (1), 31–38. https://doi.org/10.1007/s00418-010-0716-8.

Chen, Y., Zhao, Y., Chen, W., Xie, L., Zhao, Z.A., Yang, J., Chen, Y., Lei, W., Shen, Z., 2017. MicroRNA-133 overexpression promotes the therapeutic efficacy of mesenchymal stem cells on acute myocardial infarction. Stem Cell Res Ther 8 (1). https://doi.org/10.1186/S13287-017-0722-Z.

De Marchi, E., Orioli, E., Dal Ben, D., Adinolfi, E., 2016. P2X7 Receptor as a Therapeutic Target. Adv. Protein Chem. Struct. Biol. 104, 39–79. https://doi.org/10.1016/BS.APCSB.2015.11.004.

Dobaczewski, M., Bujak, M., Li, N., Gonzalez-Quesada, C., Mendoza, L.H., Wang, X.F., Frangogiannis, N.G., 2010. Smad3 Signaling Critically Regulates Fibroblast Phenotype and Function in Healing Myocardial Infarction. Circ. Res. 107 (3), 418–428. https://doi.org/10.1161/CIRCRESAHA.109.216101.

Donnelly-Roberts, D.L., Jarvis, M.F., 2007. Discovery of P2X7 receptor-selective antagonists offers new insights into P2X7 receptor function and indicates a role in chronic pain states. Br. J. Pharmacol. 151 (5), 571–579. https://doi.org/10.1038/sj.bjp.0707265.

Eltzschig, H.K., Sitkovsky, M.V., Robson, S.C., 2012. Purinergic signaling during inflammation. N. Engl. J. Med. 367 (24), 2322–2333. https://doi.org/10.1056/NEJMRA1205750.

Frangogiannis, N.G., 2015. Pathophysiology of Myocardial Infarction. Compr. Physiol. 5 (4), 1841–1875. https://doi.org/10.1002/CPHY.C150006.

Gao, H., Yin, J., Shi, Y., Hu, H., Li, X., Xue, M., Cheng, W., Wang, Y., Li, X., Li, Y., Wang, Y., Yan, S., 2017. Targeted P2X7R shRNA delivery attenuates sympathetic nerve sprouting and ameliorates cardiac dysfunction in rats with myocardial infarction. Cardiovasc. Ther. 35 (2) https://doi.org/10.1111/1755-5922.12245.

Gomez, L., Paillard, M., Thibault, H., Derumeaux, G., Ovize, M., 2008. Inhibition of GSK3beta by postconditioning is required to prevent opening of the mitochondrial permeability transition pore during reperfusion. Circulation 117 (21), 2761–2768. https://doi.org/10.1161/CIRCULATIONAHA.107.755066.

Guo, Y., Gupte, M., Umbarkar, P., Singh, A.P., Sui, J.Y., Force, T., Lal, H., 2017. Entanglement of GSK-3β, β-catenin and TGF-β1 signaling network to regulate myocardial fibrosis. J. Mol. Cell. Cardiol. 110, 109–120. https://doi.org/10.1016/J.YJMCC.2017.07.011.

Halim, S.A.S.A., Ghafar, N.A., Jubri, Z., Das, S., 2018. Induction of myocardial infarction in experimental animals: A review. J. Clin. Diagn. Res. 12 (11) https://doi.org/10.7860/JCDR/2018/36997.12221.

Honore, P., Donnelly-Roberts, D., Namovic, M.T., Hsieh, G., Zhu, C.Z., Mikusa, J.P., Hernandez, G., Zhong, C., Gauvin, D.M., Chandran, P., Harris, R., Medrano, A.P., Carroll, W., Marsh, K., Sullivan, J.P., Faltynek, C.R., Jarvis, M.F., 2006. A-740003 [N-(1-{[(cyanoimino)(5-quinolinylamino) methyl]amino}-2,2-dimethylpropyl)-2-(3,4-dimethoxyphenyl)acetamide], a novel and selective P2X7 receptor antagonist, dose-dependently reduces neuropathic pain in the rat. J. Pharmacol. Exp. Therap. 319 (3), 1376–1385. https://doi.org/10.1124/JPET.106.111559.

Ji, X., Naito, Y., Weng, H., Endo, K., Ma, X., Iwai, N., 2012. P2X7 deficiency attenuates hypertension and renal injury in deoxycorticosterone acetate-salt hypertension. Am. J. Physiol. Renal Physiol. 303 (8), F1207–F1215. https://doi.org/10.1152/ajprenal.00051.2012.

Jiang, J., Gu, X., Wang, H., Ding, S., 2021. Resveratrol improves cardiac function and left ventricular fibrosis after myocardial infarction in rats by inhibiting NLRP3 inflammasome activity and the TGF- β 1/SMAD2 signaling pathway. PeerJ 9. https://doi.org/10.7717/PEERJ.11501.

Kemp, M., Donovan, J., Higham, H., Hooper, J., 2004. Biochemical markers of myocardial injury. Br. J. Anaesth. 93 (1), 63–73. https://doi.org/10.1093/BJA/AEH148.

Khadse, N.A., Wankhade, A.M., Gaiki, A.G., 2020. Myocardial Infraction: Etiology, Risk Factors, Pathophysiology, Diagnosis and Management. American J. PharmTech Res. 10 (1), 173–190. https://doi.org/10.46624/AJPTR.2020.V10.I1.014.

Khalil, H., Kanisicak, O., Prasad, V., Correll, R.N., Fu, X., Schips, T., Vagnozzi, R.J., Liu, R., Huynh, T., Lee, S.J., Karch, J., Molkentin, J.D., 2017. Fibroblast-specific TGF-β-Smad2/3 signaling underlies cardiac fibrosis. J. Clin. Invest. 127 (10), 3770–3783. https://doi.org/10.1172/JCI94753.

Konstandin, M.H., Toko, H., Gastelum, G.M., Quijada, P., De La Torre, A., Quintana, M., Collins, B., Din, S., Avitabile, D., Völkers, M., Gude, N., Fässler, R., Sussman, M.A., 2013. Fibronectin is essential for reparative cardiac progenitor cell response after myocardial infarction. Circ. Res. 113 (2), 115–125. https://doi.org/10.1161/CIRCRESAHA.113.301152.

Laemmli, U.K., 1970. Cleavage of structural proteins during the assembly of the head of bacteriophage T4. Nature 227 (5259), 680–685. https://doi.org/10.1038/227680a0.

Lal, H., Ahmad, F., Zhou, J., Yu, J.E., Vagnozzi, R.J., Guo, Y., Yu, D., Tsai, E.J., Woodgett, J., Gao, E., Force, T., 2014. Cardiac fibroblast glycogen synthase kinase-3β regulates ventricular remodeling and dysfunction in ischemic heart. Circulation 130 (5), 419–430. https://doi.org/10.1161/CIRCULATIONAHA.113.008364.

Lal, H., Ahmad, F., Woodgett, J., Force, T., 2015. The GSK-3 family as therapeutic target for myocardial diseases. In *Circulation Research*, Vol. 116, Issue 1. Circ. Res., pp. 138–149 Doi: 10.1161/CIRCRESAHA.116.303613.

Li, C., Meng, X., Wang, L., Dai, X., 2023. Mechanism of action of non-coding RNAs and traditional Chinese medicine in myocardial fibrosis: Focus on the TGF-β/Smad signaling pathway. Front. Pharmacol. 14 https://doi.org/10.3389/FPHAR.2023.1092148.

Liles, J.H., Flecknell, P.A., 1992. The use of non-steroidal anti-inflammatory drugs for the relief of pain in laboratory rodents and rabbits. Lab. Anim 26 (4), 241–255. https://doi.org/10.1258/002367792780745706.

Liu, J., Li, G., Peng, H., Tu, G., Kong, F., Liu, S., Gao, Y., Xu, H., Qiu, S., Fan, B., Zhu, Q., Yu, S., Zheng, C., Wu, B., Peng, L., Song, M., Wu, Q., Li, G., Liang, S., 2013. Sensory-sympathetic coupling in superior cervical ganglia after myocardial ischemic injury facilitates sympathoexcitatory action via P2X7 receptor. Purinergic Signalling 9 (3), 463–479. https://doi.org/10.1007/S11302-013-9367-2.

Lovelock, J.D., Baker, A.H., Gao, F., Dong, J.F., Bergeron, A.L., McPheat, W., Sivasubramanian, N., Mann, D.L., 2005. Heterogeneous effects of tissue inhibitors of matrix metalloproteinases on cardiac fibroblasts. Am. J. Physiol. Heart Circ. Physiol. 288 (2 57–2), 461–468. https://doi.org/10.1152/AJPHEART.00402.2004/ASSET/IMAGES/LARGE/ZH40020536270006.JPEG.

Martin, T.P., MacDonald, E.A., Elbassioni, A.A.M., O'Toole, D., Zaeri, A.A.I., Nicklin, S. A., Gray, G.A., Loughrey, C.M., 2022. Preclinical models of myocardial infarction: from mechanism to translation. Br. J. Pharmacol. 179 (5), 770–791. https://doi.org/10.1111/bph.15595.

Mechanic, O.J., Gavin, M., Grossman, S. A., 2022, August 8. *Acute Myocardial Infarction - StatPearls - NCBI Bookshelf*. StarPearls. https://www.ncbi.nlm.nih.gov/books/NBK459269/.

Mezzaroma, E., Toldo, S., Farkas, D., Seropian, I. M., Van Tassell, B. W., Salloum, F. N., Kannan, H. R., Menna, A. C., Voelkel, N. F., Abbate, A., 2011. The inflammasome promotes adverse cardiac remodeling following acute myocardial infarction in the mouse. *Proc. Nat. Acad. Sci. USA 108*(49), 19725–19730. Doi: 10.1073/pnas.1108586108.

Michaud, K., Basso, C., d'Amati, G., Giordano, C., Kholová, I., Preston, S.D., Rizzo, S., Sabatasso, S., Sheppard, M.N., Vink, A., van der Wal, A.C., 2020. Diagnosis of myocardial infarction at autopsy: AECVP reappraisal in the light of the current clinical classification. Virchows Arch. 476 (2), 179–194. https://doi.org/10.1007/S00428-019-02662-1/FIGURES/7.

Monção-Ribeiro, L.C., Faffe, D.S., Santana, P.T., Vieira, F.S., da Graça, C.L.A.L., Marques-da-Silva, C., Machado, M.N., Caruso-Neves, C., Zin, W.A., Borojevic, R., Takiya, C. M., Coutinho-Silva, R., 2014. P2X7 receptor modulates inflammatory and functional pulmonary changes induced by silica. PLoS One 9 (10), e110185.

Musa, H., Tellez, J.O., Chandler, N.J., Greener, I.D., Mączewski, M., MacKiewicz, U., Beresewicz, A., Molenaar, P., Boyett, M.R., Dobrzynski, H., 2009. P2 purinergic receptor mRNA in rat and human sinoatrial node and other heart regions. Naunyn-Schmiedeberg's Arch. Pharmacol. 379 (6), 541–549. https://doi.org/10.1007/S00210-009-0403-2.

Nicin, L., Wagner, J.U.G., Luxán, G., Dimmeler, S., 2022. Fibroblast-mediated intercellular crosstalk in the healthy and diseased heart. FEBS Lett. 596 (5), 638–654. https://doi.org/10.1002/1873-3468.14234.

North, R.A., 2002. Molecular physiology of P2X receptors. Physiol. Rev. 82 (4), 1013–1067. https://doi.org/10.1152/PHYSREV.00015.2002.

Ortega, F., Pérez-Sen, R., Morente, V., Delicado, E.G., Miras-Portugal, M.T., 2010. P2X7, NMDA and BDNF receptors converge on GSK3 phosphorylation and cooperate to promote survival in cerebellar granule neurons. Cell. Mol. Life Sci. 67 (10), 1723. https://doi.org/10.1007/S00018-010-0278-X.

Qiu, H., Liu, W., Lan, T., Pan, W., Chen, X., Wu, H., Xu, D., 2018. Salvianolate reduces atrial fibrillation through suppressing atrial interstitial fibrosis by inhibiting TGF-β1/Smad2/3 and TXNIP/NLRP3 inflammasome signaling pathways in post-MI rats. Phytomedicine 51, 255–265. https://doi.org/10.1016/J.PHYMED.2018.09.238.

Sandanger, Ø., Ranheim, T., Vinge, L.E., Bliksøen, M., Alfsnes, K., Finsen, A.V., Dahl, C. P., Askevold, E.T., Florholmen, G., Christensen, G., Fitzgerald, K.A., Lien, E., Valen, G., Espevik, T., Aukrust, P., Yndestad, A., 2013. The NLRP3 inflammasome is up-regulated in cardiac fibroblasts and mediates myocardial ischaemia-reperfusion injury. Cardiovasc. Res. 99 (1), 164–174. https://doi.org/10.1093/cvr/cvt091.

Shinde, A.V., Humeres, C., Frangogiannis, N.G., 2017. The role of α-smooth muscle actin in fibroblast-mediated matrix contraction and remodeling. Biochim. Biophys. Acta (BBA) - Mol. Basis Dis. 1863 (1), 298–309. https://doi.org/10.1016/J.BBADIS.2016.11.006.

Shokoples, B.G., Paradis, P., Schiffrin, E.L., 2021a. P2X7 Receptors: An Untapped Target for the Management of Cardiovascular Disease. Arterioscler. Thromb. Vasc. Biol. 41 (1), 186–199. https://doi.org/10.1161/ATVBAHA.120.315116.

Shokoples, B.G., Paradis, P., Schiffrin, E.L., 2021b. P2X7 Receptors. Arterioscler. Thromb. Vasc. Biol. 41 (1), 186–199. https://doi.org/10.1161/ATVBAHA.120.315116.

Sutton, N.R., Hayasaki, T., Hyman, M.C., Anyanwu, A.C., Liao, H., Petrovic-Djergovic, D., Badri, L., Baek, A.E., Walker, N., Fukase, K., Kanthi, Y., Visovatti, S.H., Horste, E.L., Ray, J.J., Goonewardena, S.N., Pinsky, D.J., 2017. Ectonucleotidase CD39-driven control of postinfarction myocardial repair and rupture. JCI Insight 2 (1). https://doi.org/10.1172/jci.insight.89504.

Tu, G., Li, G., Peng, H., Hu, J., Liu, J., Kong, F., Liu, S., Gao, Y., Xu, C., Xu, X., Qiu, S., Fan, B., Zhu, Q., Yu, S., Zheng, C., Wu, B., Peng, L., Song, M., Wu, Q., Liang, S., 2013. P2X(7) inhibition in stellate ganglia prevents the increased sympathoexcitatory reflex via sensory-sympathetic coupling induced by myocardial ischemic injury. Brain Res. Bull. 96, 71–85. https://doi.org/10.1016/J.BRAINRESBULL.2013.05.004.

Tung, H.-C., Lee, F.-Y., Wang, S.-S., Tsai, M.-H., Lee, J.-Y., Huo, T.-I., Huang, H.-C., Chuang, C.-L., Lin, H.-C., Lee, S.-D., 2015. The Beneficial Effects of P2X7 Antagonism in Rats with Bile Duct Ligation-induced Cirrhosis. PLoS One 10 (5), e0124654.

Verkhratsky, A., Burnstock, G., 2014. Biology of purinergic signalling: its ancient evolutionary roots, its omnipresence and its multiple functional significance. Bioessays 36 (7), 697–705. https://doi.org/10.1002/BIES.201400024.

Webb, I.G., Nishino, Y., Clark, J.E., Murdoch, C., Walker, S.J., Makowski, M.R., Botnar, R.M., Redwood, S.R., Shah, A.M., Marber, M.S., 2010a. Constitutive glycogen synthase kinase-3alpha/beta activity protects against chronic beta-

adrenergic remodelling of the heart. Cardiovasc. Res. 87 (3), 494–503. https://doi.org/10.1093/CVR/CVQ061.

Webb, I.G., Sicard, P., Clark, J.E., Redwood, S., Marber, M.S., 2010b. Myocardial stress remodelling after regional infarction is independent of glycogen synthase kinase-3 inactivation. J. Mol. Cell. Cardiol. 49 (5), 897–900. https://doi.org/10.1016/j.yjmcc.2010.07.021.

WHO, 2018. *Noncommunicable diseases country profiles*. Retrieved August 8, 2021. From; World Health Organization. https://apps.who.int/iris/handle/10665/274512.

WHO, 2021, June 11. *Cardiovascular diseases (CVDs) fact sheet*. Retrieved August 8, 2021. From. https://www.who.int/news-room/fact-sheets/detail/cardiovascular-diseases-(cvds).

Woulfe, K.C., Gao, E., Lal, H., Harris, D., Fan, Q., Vagnozzi, R., Decaul, M., Shang, X., Patel, S., Woodgett, J.R., Force, T., Zhou, J., 2010. Glycogen synthase kinase-3beta regulates post-myocardial infarction remodeling and stress-induced cardiomyocyte proliferation in vivo. Circ. Res. 106 (10), 1635–1645. https://doi.org/10.1161/CIRCRESAHA.109.211482.

Yin, J., Wang, Y., Hu, H., Li, X., Xue, M., Cheng, W., Wang, Y., Li, X., Yang, N., Shi, Y., Yan, S., 2017a. P2X7 receptor inhibition attenuated sympathetic nerve sprouting after myocardial infarction via the NLRP3/IL-1β pathway. J. Cell Mol. Med. 21 (11), 2695. https://doi.org/10.1111/JCMM.13185.

Yin, X., Yin, X., Pan, X., Zhang, J., Fan, X., Li, J., Zhai, X., Jiang, L., Hao, P., Wang, J., Chen, Y., 2023. Post-myocardial infarction fibrosis: Pathophysiology, examination, and intervention. Front. Pharmacol. 14 https://doi.org/10.3389/FPHAR.2023.1070973/FULL.

Yin, J., You, S., Liu, H., Chen, L., Zhang, C., Hu, H., Xue, M., Cheng, W., Wang, Y., Li, X., Shi, Y., Li, N., Yan, S., Li, X., 2017b. Role of P2X7R in the development and progression of pulmonary hypertension. Respir. Res. 18 (1) https://doi.org/10.1186/S12931-017-0603-0.

Zapata-Sudo, G., da Silva, J.S., Pereira, S.L., Souza, P.J.C., de Moura, R.S., Sudo, R.T., 2014. Oral treatment with Euterpe oleracea Mart. (açaí) extract improves cardiac dysfunction and exercise intolerance in rats subjected to myocardial infarction. BMC Complement. Altern. Med. 14 https://doi.org/10.1186/1472-6882-14-227.

Zempo, H., Sugita, Y., Ogawa, M., Watanabe, R., Suzuki, J.I., Isobe, M., 2015. A P2X7 receptor antagonist attenuates experimental autoimmune myocarditis via suppressed myocardial CD4+ T and macrophage infiltration and NADPH oxidase 2/4 expression in mice. Heart Vessels 30 (4), 527–533. https://doi.org/10.1007/S00380-014-0527-2.

Zhang, Y., Cheng, H., Li, W., Wu, H., Yang, Y., 2019. Highly-expressed P2X7 receptor promotes growth and metastasis of human HOS/MNNG osteosarcoma cells via PI3K/Akt/GSK3β/β-catenin and mTOR/HIF1α/VEGF signaling. Int. J. Cancer 145 (4), 1068–1082. https://doi.org/10.1002/ijc.32207.

Zhao, W., Zhao, J., Rong, J., 2020. Pharmacological Modulation of Cardiac Remodeling after Myocardial Infarction. In: Oxidative Medicine and Cellular Longevity. Hindawi Limited. https://doi.org/10.1155/2020/8815349.

Zhou, J., Tian, G., Quan, Y., Li, J., Wang, X., Wu, W., Li, M., Liu, X., Liu, X., 2020. Inhibition of P2X7 Purinergic Receptor Ameliorates Cardiac Fibrosis by Suppressing NLRP3/IL-1 β Pathway. Oxid. Med. Cell. Longev. 2020 https://doi.org/10.1155/2020/7956274.